PROOF OF CONCEPT OF A BRILLOUIN-LIDAR FOR REMOTE SENSING OF OCEANIC TEMPERATURE PROFILES

Alexandru Popescu[1], Kai Schorstein[1] and Thomas Walther[1]

1. TU Darmstadt, Institute for Applied Physics, Schlossgartenstr. 7, D-64289 Darmstadt, Germany, http://www.lqo.tu-darmstadt.de, thomas.walther@physik.tu-darmstadt.de

ABSTRACT

A remote sensing technique measuring temperature profiles of the upper-ocean mixed layer would provide valuable input to climate studies, weather forecasts and oceanography in general. Originally proposed by Hirschberg et al., later demonstrated by Guagliardo et al. using pulsed lasers and Hirschberg et al. using cw-lasers, the working principle is an extension to common airborne lidar bathymetry. Light sent into the Ocean undergoes a Brillouin shift leading to additional frequency components in the back-scattered light. Specifically, the injected laser pulses are scattered off of moving density fluctuations in the water; due to the Doppler shift, the spectrum of the back-scattered light is shifted to the red and blue of the original light frequency. Typical frequency shifts to be expected are in the order of 7-8 GHz located symmetrically around the wavelength of the laser pulses. The shift is proportional to the local speed of sound and the index of refraction, and thus a function of temperature. Therefore, temperature information can be extracted. The temperature profile can be deduced by the timing information.

In our approach, the intended light source is comprised of a three-stage pulsed Yb-doped fiber amplifier frequency doubled into the green spectral range. Using this laser system we succeeded in performing the first temperature measurements employing a frequency-doubled fiber amplifier. Furthermore, we performed first range resolved measurements in our laboratory set-up demonstrating the proof of concept for a Brillouin lidar system. In these measurements we used a Fabry-Perot etalon as the detector for the Brillouin shifts, which cannot be used in a practical implementation due to restrictions in light gathering power and susceptibility to vibrations.

Instead we propose an excited state Faraday anomalous dispersion optical filter (ESFADOF) approach for a practical system. ESFADOFs allow the implementation of flexible edge filters. Edge filters with steep transmission edges in the regions of interest convert small frequency shifts in the Brillouin lines to a relatively large change of transmission. By exploiting the anomalous dispersion in the vicinity of an atomic transition, their filter characteristics can be tuned over a wide range and can be tailored to meet the required filter characteristics. In addition the filter shows excellent suppression of background, i.e. day light.

1 INTRODUCTION

The knowledge of temperature profiles of the upper-ocean mixed layer is highly relevant to oceanography. Furthermore, this data can give valuable input to climate studies and weather forecasts. Currently, the measurement of temperature profiles is based on in-situ techniques such as fixed buoys or bathythermographs, that are deployed from aircrafts or ships. However, these techniques cannot deliver cost-effective on-line data from an extended region of the ocean. The exploitation of spontaneous Brillouin scattering in the water for measuring sound speed and water temperature was proposed by Guagliardo et al ([1]). In combination with the remote sensing lidar technique, a powerful instrument results, which provides a supplementary, more efficient technique compared to established in situ techniques. In general, the lidar working principle is straight forward: A laser pulse is sent into the water. In the water Brillouin scattering occurs and the backscattered light is analyzed by the detector. Then, the temperature information is extracted from the signal and a depth resolution is realized by a time of flight correlation. Specifically, light propagating in water is scattered off of moving density fluctuations in the water; due to the Doppler shift the spectrum of the backscattered light shows components shifted to the red and blue of the original light frequency. Thus, the method is sensitive to the local velocity of sound. The shifted frequency components are referred to as Brillouin lines.

Typical frequency shifts for 532 nm-light to be expected for water temperatures and salinities found in the oceans are in the order of 7-8 GHz ([2]). As the dependence of the shift on temperature is known, the temperature information can be extracted from the data. Specifically, the relation between the Brillouin shift ν_B and the velocity of sound v_s for backscattered light is given by

$$\nu_B = \pm 2 \frac{n(S,T,\lambda) v_s(S,T)}{\lambda} \tag{1}$$

The dependence of the refractive index $n(S,T,\lambda)$ and of the sound velocity $v_s(S,T)$ on the salinity S, the temperature T and the wavelength λ are well known ([2]). Relying on historical data for the salinity S and measuring the Brillouin shift ν_B enables us to deduce the temperature T. It should be noted that there is also a dependence on pressure p, which has been omitted for clarity in the above equation. It could be easily taken into account ([2]).

Laboratory based measurements by Fry and coworkers have shown the feasibility of this approach ([3–5]). Theoretical investigations of the accuracy limitations have been performed. It was found that an uncertainty of 1 MHz in the frequency shift measurement corresponds to an uncertainty in the temperature of 0.06°C when the salinity is known. Assuming a world-wide constant salinity, averaged over historical data, a temperature accuracy of 0.5°C is possible with a frequency uncertainty of 4 MHz ([2]). The reachable depth is limited by the available laser power, the detector sensitivity, the detector dynamic range, the signal-to-noise ratio and the absorption in water. Estimates result in a penetration depth of up to 100 m ([6]). The spatial resolution in the water is about a meter for pulse durations of 10 ns.

The necessary minimum specifications of the complete sensor system are rather stringent: (1) Since operation from a mobile platform is intended, the entire sensor has to be compact, insensitive to vibrations and exhibit low power consumption. (2) In order to resolve the Brillouin-shift the laser source has to produce relatively high energy ns-pulses, preferentially near-Fourier transform limited. (3) The laser radiation should be close to the absorption minimum of water, i.e. between 380 and 550 nm ([7]). (4) The receiver unit must exhibit a high light gathering power, and be able to resolve the Brillouin-shift.

As proposed in earlier publications ([8–12]) a light source which is compatible with the specifications is a pulsed fiber amplifier. The fiber amplifier is composed of a master oscillator (seed) which defines spectral and temporal properties of the light and a power amplifier. Since the power amplifier does not need any resonant optics, the system is intrinsically less sensitive to vibrations.

Different concepts for detecting the frequency shift are possible. The most straight forward solution is a scanning Fabry-Perot interferometer, which is perfectly suited in a laboratory frame. Carefully built, it possesses the required frequency resolution and the position of the Brillouin shifted lines can be accurately measured. But since scanning interferometers have not enough light gathering power and are sensitive to vibrations, better suited detection concepts such as edge filter techniques or heterodyne detection have to be considered.

We are favoring an edge filter technique with steep transmission changes at the desired frequency range of ±7-8 GHz transforming the frequency shift into a change of transmission. Excited State Faraday Anomalous Dispersion Optical Filters (ESFADOF) are such static devices which are able to generate these steep transmission changes without the problems of stability and light gathering power.

All the Brillouin-spectra measurements which are presented in the following chapter were still performed with a scanning Fabry-Perot interferometer. However, an additional chapter is dedicated to the ESFADOF concept documenting the current status of development. The ESFADOF will be integrated into the whole system in the near future replacing the FPI detector.

2 THE LIGHT SOURCE: A FIBER AMPLIFIER

Operation from a mobile platform such as an airplane or a helicopter is intended. Therefore the whole system has to be rather rugged in order to cope with the vibrationally challenging environment. A fiber amplifier is based on non resonant techniques and therefore exhibits a relatively low sensitivity to vibration. Disturbance of the amplifier operation affects the output energy, but not the spectral and temporal properties of the radiation. Due to its large surface-to-volume ratio the cooling requirements are reduced. Furthermore, the fiber amplifier concept complies with the boundary conditions concerning weight (<300 kg), dimension and electrical power consumption (<2 kW) which are essential for a practical implementation of the lidar system ([13]).

Fiber amplifiers and fiber laser have been increasingly successful in recent decades. Especially the Yb-ion has been of particular interest for high power applications ([14,15]). Yb-doped fiber amplifiers and lasers have proven their enormous flexibility. Nevertheless, the development has been focused predominantly on power scaling in order to close the gap to competing rod or disc type laser geometries. Double clad fibers have been introduced in order to use low brightness high power pump diodes ([16,17]). The large mode area design with low numerical aperture allows the power scaling while maintaining a good beam profile ([18]). Usually power scaling is achieved by sacrificing the spectral properties, i.e. spectral bandwidth. Using such a technique a 4-ns pulsed fiber laser with 2.4 MW peak power has been demonstrated ([19]). Recently, a Q-switched output with 2-mJ output has been achieved ([20]).

For our lidar application laser pulses with durations of 10 ns are desired, corresponding to a spatial temperature resolution of approximately 1 m in water. The temperature measurement accuracy is influenced by the frequency resolution demanding for Fourier transform limited pulses. The combination of high power and narrow linewidth represents the challenge in the design of the fiber amplifier.

2.1 Experimental Set-up

Due to the flexibility of fiber amplifiers, we opted for a home-built frequency doubled Yb-doped fiber amplifier. The system is a very versatile light source for small bandwidth radiation in the wavelength region between 1030 and 1100 nm, covered by the Yb-ion when pumped with 976 nm-light. The set-up of the three-stage fiber amplifier is depicted in fig. 1 and has been already discussed in detail in ref. ([21]). Here, we only reiterate the main specifications. The design allows continuous wave as well as pulsed operation with flexible pulse durations between 10 ns to 1200 ns and repetition rates of up to 5 kHz. The seed source delivers low energy seed pulses with the desired pulse width, wavelength and bandwidth. By cutting out laser pulses using an electro optic modulator (EOM), the bandwidth of the 10 ns pulses is given by the Fourier-transform of the temporal pulse shape ([22]). The seed pulses are amplified by three consecutive amplification stages, which are similar in configuration, but differ in fiber lengths and geometry as well as the pump laser employed. The schematic in fig. 1 shows all three stages. In addition, table 1 compiles the individual fiber properties. Between each amplification stage band pass filters and Faraday isolators are placed to block unwanted radiation which might propagate backwards through the stages.

The operation of a fiber amplifier with ns-pulses with near Fourier-transform limited bandwidth is especially challenging. The high light intensity which is reached over the rather long interaction length of the fiber promotes the onset of nonlinear effects. In particular, the extreme small bandwidth of the Fourier-transform limited pulses support the onset of stimulated Brillouin scattering (SBS) ([23,24]). In general, the threshold for SBS depends on the intensity, the fiber length, the pulse duration and bandwidth of the radiation as well as pump geometry. Our selection of fibers (cf. table 1) represents an optimization regarding high SBS threshold which results in high output energy while maintaining a relatively good beam profile and a good polarization ratio ([21]). These parameters are crucial for the final second harmonic generation process. All stages are pumped in a counter-propagating configuration because this increases the SBS threshold, by reducing the ratio between average energy along the fiber compared to the output energy of the stage ([25]).

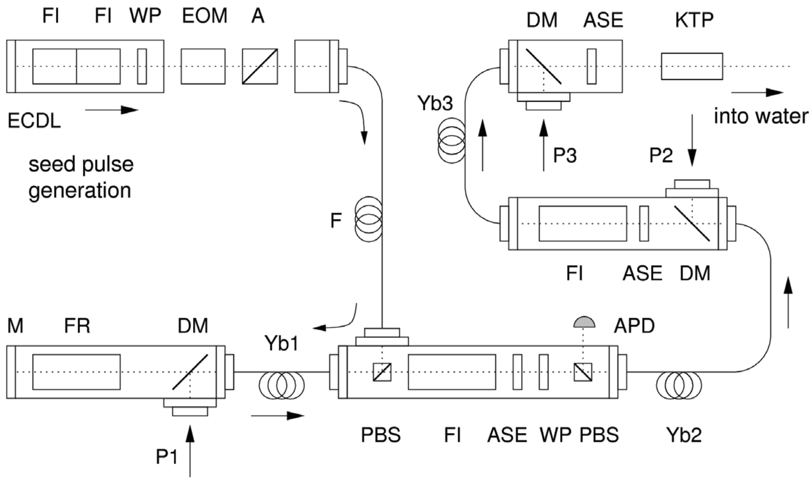

Figure 1: Set-up of the fiber amplifier: Yb-doped fibers (Yb1-3), patch fiber (F), seed laser (ECDL), pump lasers (P1-3), electro-optic modulator (EOM), polarizer (P), analyzer (A), polarizing beam splitter (PBS), mirror (M), Faraday isolator (FI), Faraday rotator (FR), λ/2-wave plate (WP), dichroic mirror (DM), interference filters (ASE) and avalanche photo diode (APD) for detection of the SBS threshold.

Table 1: Fiber properties of the Yb-doped fibers of all three amplification stages. This is the result of the optimization procedure regarding high SBS threshold which results in high output energy while maintaining a good beam profile and a good polarization ratio.

Stage	**1**	**2**	**3**
core diameter	4.4 µm	28 µm	55 µm
pump core diameter	–	400 µm	400 µm
NA core	0.15	0.06	0.19
NA pump core	–	0.38	0.38
fiber length	1.3 m	12.5 m	0.67 m
Yb concentration	6500 ppm	500 ppm	6500 ppm
V-number	1.95	4.96	30.8
guided modes	1	10	390

A second harmonic generation unit based on a KTP crystal is used in order to reach the green spectral region of 515 - 550 nm. This large tuning range of the fiber amplifier is advantageous in order to match the operation wavelength to the requirements of the intended detector based on an ESFADOF presented in section 4 ([10]).

2.2 Results

The fiber amplifier has been completely characterized at an operation wavelength of 1064 nm, a pulse duration of 10 ns at a repetition rate of 1 kHz and was operated well below the SBS threshold. The SBS threshold for each stage has been determined individually using the method described in ref. ([21]). Operation above the SBS threshold is not desirable since it reduces the output energy stability, may produce multiple output pulses and ultimately may damage the fiber end facets. After the third stage the amplifier delivers up to 516 µJ per pulse limited by the onset of SBS. After second harmonic generation, an energy of 131 µJ per pulse at 532 nm is available. The total gain of all three amplifier stages is 61.9 dB. The Fourier-transform limited bandwidth is reached within a factor of 1.01(7) and has been determined by relating the optical bandwidth to the pulse duration. The bandwidth was measured with a slowly scanning Fabry-Perot interferometer with a free spectral range of 1 GHz. Due to amplification and second harmonic generation the pulse duration is reduced to 7.7 ns. Long-term frequency and energy stability are more than sufficient for Brillouin lidar experiments.

3 RANGE RESOLVED MEASUREMENTS OF THE WATER TEMPERATURE

In a next step we performed range resolved measurements of a water temperature distribution employing the lidar technique in a laboratory set-up. For this task we implemented an experimental set-up consisting of the light source described above, a water filled tube and a Fabry Perot detector system (cf. fig. 2 and 4b). For the following measurements, the fiber amplifier delivered optical pulses with a pulse duration of 7.7 ns, an energy of 36.9 µJ at a repetition rate of 5 kHz ([26]).

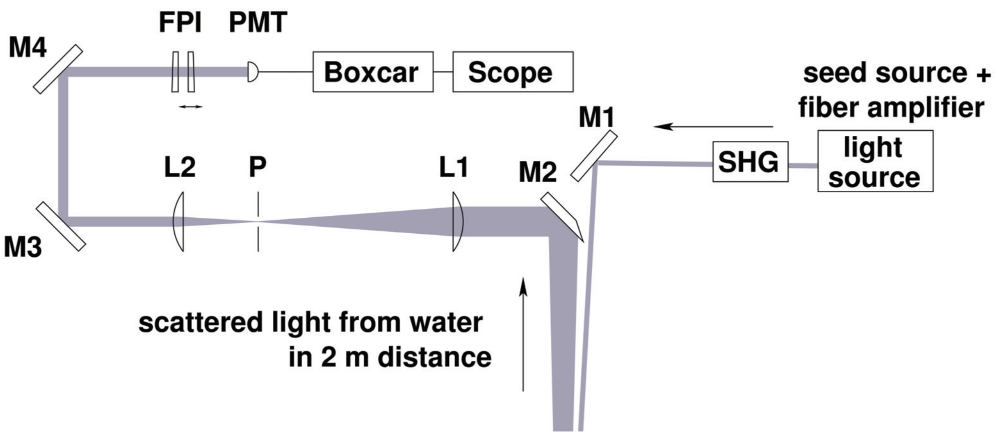

Figure 2: Schematic of the transmitting and receiving optics: Mirrors (M1-4), pinhole P, lenses L1,L2, plane Fabry-Perot interferometer (FPI), photo multiplier (PMT) and boxcar averager (Boxcar).

3.1 Experimental Set-up

The water filled tube consists of two segments which can be independently temperature stabilized to values between 4°C and 38°C. It is placed in a horizontal orientation as shown in fig. 4b and is filled with double distilled water with zero salinity. A micro filter and a UV-C light source are used to remove particles and to suppress the growth of algae. All glass windows of the water tube are inclined at 3° in order to reduce Fresnel reflection effects. As indicated in fig. 4b, the water flows from the middle of the segments to both ends in order to maintain a large temperature gradient. Thermocouples are inserted from the top to measure the water temperature in each of the segments.

The output of the fiber amplifier is directed into the water by the mirror M1 of the transmission and receiving optics shown in fig. 2. The mirror M2 is a D-shaped mirror in order to minimize the angle between the transmission beam and the back-scattered light that is collected by the telescope (L1, L2) and directed towards the scanning Fabry-Perot interferometer (FPI) by mirrors (M3, M4). The telescope reduces the size of the backscattered beam by a factor of 2.5. The pinhole P and the lens L1 define the detection volume. Finally, the light is detected by a photo multiplier (PMT). The depth of the actual measurement is defined by the electronic delay of the boxcar averager (Boxcar) and corresponds to the time of flight of the laser pulse.

3.3 Results and data analysis

By slowly scanning the FPI a full spectrum of the backscattered light is recorded for a certain electronic delay corresponding to a certain depth. A typical spectrum (cf. fig. 3) is composed of large peaks which are due to elastic scattering by particles suspended in the water. These peaks are relatively large, since no particular effort beyond the micro filter was used to purify the water. The smaller peaks are due to Brillouin scattering. The frequency shift between the Brillouin- and elastic scattering peaks carries the desired temperature information. It was determined from the spectrum following the procedure outlined below. A single spectrum consists of approximately 130000 laser pulses with an applied moving average of 30. The two Brillouin peaks located symmetrically around the elastic scattering peaks originate from the two opposite directions of motion of the sound waves in the water. In order to precisely measure the frequency shift the free spectral range (FSR) of the FPI must be calibrated with high accuracy. Therefore, the fiber amplifier is switched to continuous wave operation by modifying the pulse generating unit ([27]). Its output is directed into the FPI as well as into a FPI with a known FSR of 1 GHz. By slowly scanning the ECDL that seeds the amplifier and by comparing the frequency markers of both FPIs, the unknown FSR of the FPI was determined to be 20.074(1) GHz. After the successful FPI calibration the amplifier, is switched to pulsed mode and the Brillouin spectra are recorded as indicated before.

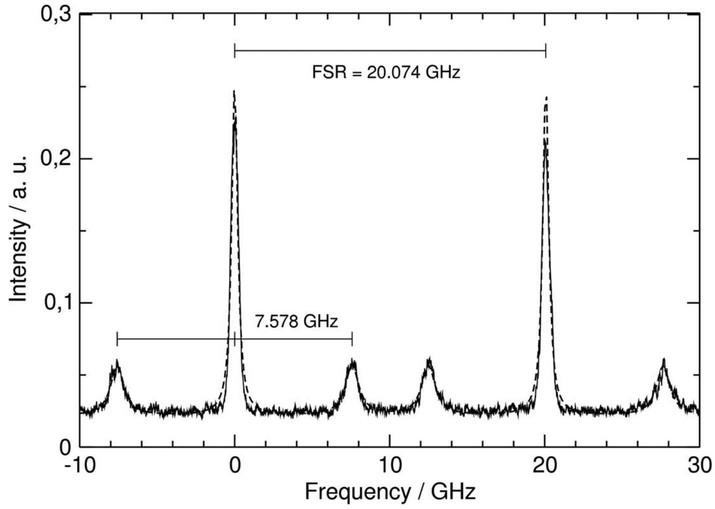

Figure 3: Calibrated Brillouin spectrum for a water temperature of 31.9(2)°C: The calibrated FSR of the FPI is 20.074(1) GHz and the measured frequency shift is 7.578(9) GHz.

The extraction of the temperature information is as follows: The frequency axes of the recorded spectra are calibrated and corrected for the non-linearity of the piezo-electric transducer in the FPI by exploiting the symmetry of the Brillouin shift with respect to the elastic scattering peak. In order to correct the non-linearities a quadratic function is sufficient. Finally, an appropriate model function consisting of Airy and Lorentz functions is fitted to the data and the frequency shift is extracted. The error is estimated by the residuals of the fitting procedure. In fig. 3 a fully calibrated spectrum for a water temperature of 31.9(2)°C is shown. It shows a frequency shift of 7.578(9) GHz. Finally, from the Brillouin shift a water temperature is determined according to the empirical relationship given in ref. ([2]). The frequency error translates into a temperature error of about 0.6°C.

The time delay between the laser pulse and the gate of the boxcar defines the water depth from which the spectrum is recorded. Thus, by varying the delay the temperature distribution can be recorded (cf. fig. 4). The two segments were temperature stabilized to temperatures of 32.4°C and 4.6°C, respectively.

In fig. 4 the result of the depth resolved measurement is shown, together with the independently measured actual water temperature while recording the spectrum. For each data point an entire spectrum comparable to that shown in fig. 3 has been recorded at the specific delay time corresponding to the appropriate distance. Clearly, the two different temperatures are reproduced accurately. The spatial resolution corresponds to approximately 1.5(2) m, this is consistent with the pulse duration of 7.7 ns and the gate width of 5 ns. The processed spectrum displayed in fig. 3 corresponds to the data point marked with a red circle in fig. 4.

These measurements demonstrate the general feasibility of our remote sensing technique using a pulsed fiber amplifier as the light source. Clearly, the detection unit based on a FPI and the employed procedure does not fulfill the stated requirements on stability and single-shot capability. The FPI will be replaced in the near future by an edge filter based on an excited state Faraday anomalous optical filter (ESFADOF) as discussed in the next section.

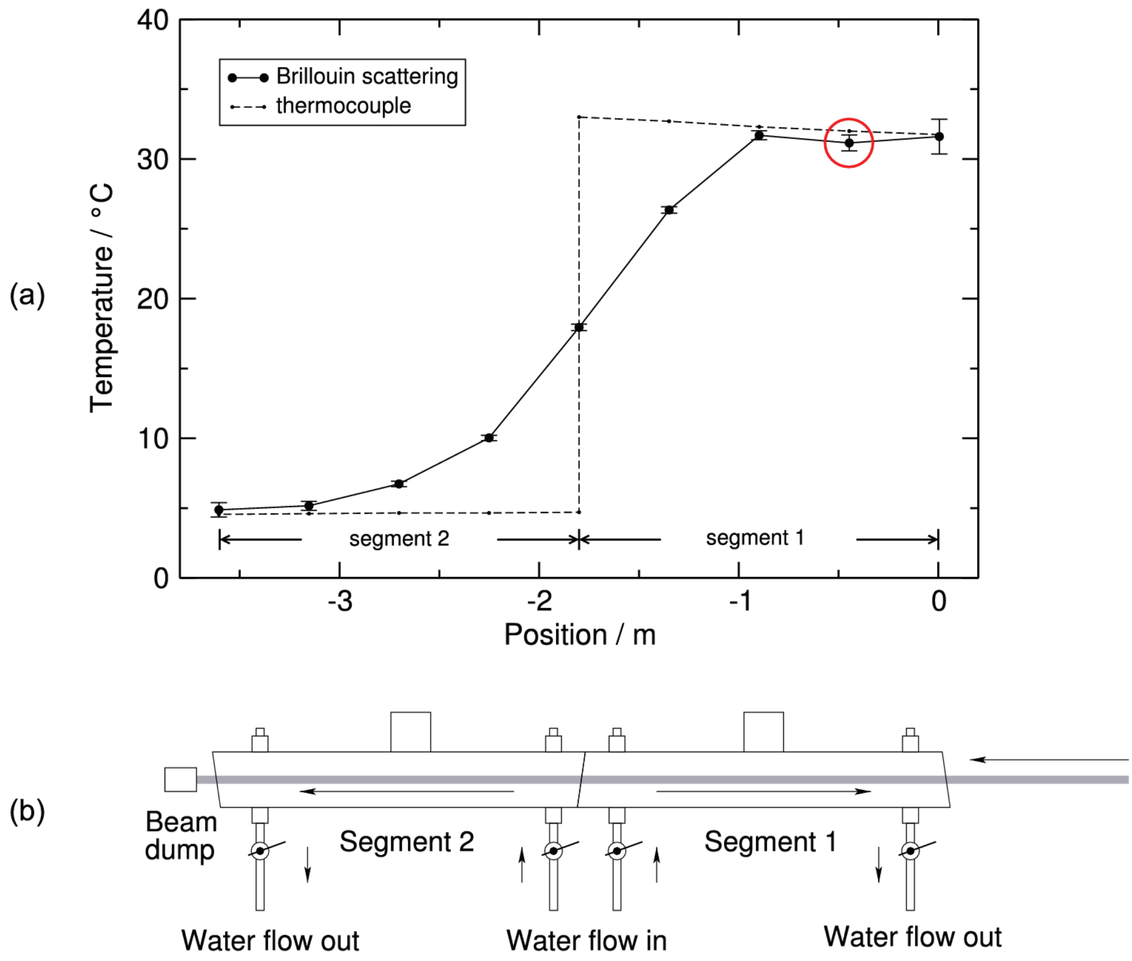

Figure 4: (a) Measured temperature distribution of the two segments held at different temperatures: The temperatures shown are measured with Brillouin scattering and additionally with a thermocouple. The temperature step is clearly visible. The broadening of the step of about 1.5(2) m is due to the pulse duration and the gate size. The circled data point corresponds to the spectrum shown in fig. 3. (b) Schematic of the water tube consisting of a two segments: The laser pulses are sent into the water from the right and hit a beam dump at the left end. The glass panes are inclined at 3°. The water flow is indicated and maximizes the temperature gradient in the middle. Thermocouples inserted from the top measure the water temperature.

4 RECEIVER

The measurement of the small Brillouin-shifts will be based on a static edge-filter, capable of transforming small frequency shifts into large changes of the transmitted intensity. The design criteria of our edge filters are: (1) Steep transmission edges, (2) symmetrically located in the spectral region of interest, i.e. ±7-8 GHz around the working wavelength, and (3) a maximum overall transmission for a sufficient signal-noise ratio. The symmetry significantly reduces the influence of laser frequency jitter. In our case an Excited state Faraday Anomalous Dispersion Optical Filter (ESFADOF) is the most promising approach. It will be briefly introduced, for a more detailed discussion on the underlying theory and the experimental set-up we refer to some of our earlier publications ([8–12,28]).

Briefly speaking Faraday anomalous dispersion optical filters (FADOFs) and their excited state counterparts ESFADOFs consist of an atomic vapor cell placed in an homogeneous magnetic field between two crossed polarizers. The working principle is as follows (cf. fig. 5): (1) The incident light is polarized by the first polarizer and (2) passes the gas cell. (3) The high anomalous dispersion of the atomic vapor in the vicinity of its absorption lines results in a wavelength dependent rotation of the polarization vector. (4) Finally, the second polarizer, which is rotated by 90° with respect to the first one, projects the polarization onto its basis, and therefore converts the rotation of the polarization into a change in the transmitted intensity. As ESFADOFs exploit atomic transitions between two excited states, an external pump source populating the lower ESFADOF state is necessary.

In order to investigate the feasibility of our ESFADOF approach, we set-up an ESFADOF and measured its transmission spectra. The set-up consists of the ESFADOF, a pump and probe laser, a spectrum calibration unit as well as several photodiodes. The probe radiation is generated by frequency doubling the output of a one staged fiber amplifier, similar to the one presented earlier, operated in cw mode. The filter characteristics of the ESFADOF has been recorded by tuning the wavelength of the ECDL seeding the fiber amplifier.

As a beneficial side effect, the two crossed polarizers exhibit an excellent daylight rejection, making the measurement intrinsically insensitive to sunlight. Furthermore, as only static mechanical components are necessary, the ESFADOF-detector is insensitive to vibrations.

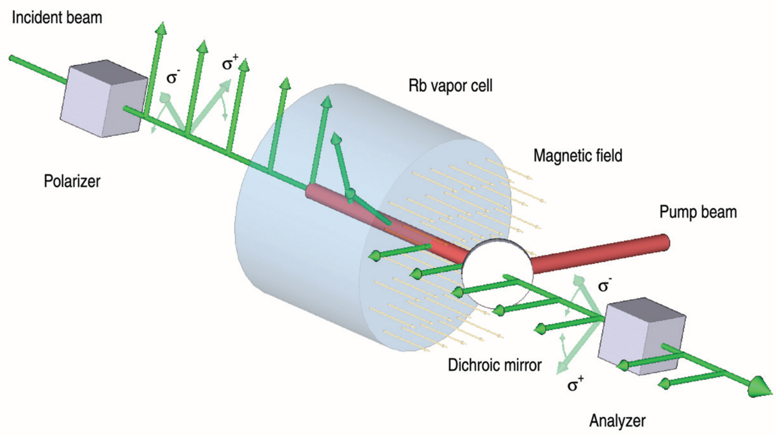

Figure 5: Schematic drawing of an ESFADOF: It consists of an atomic vapor cell placed between two crossed polarizers. Due to the presence of the magnetic field, left and right circular polarized light, σ^- and σ^+, experience in the vicinity of the atomic absorption lines wavelength dependent dispersions on their path through the vapor cell. As the dispersions differ a significant phase difference between both circular polarizations is the direct result and therefore a rotation of the polarization vector occurs. The second polarizer projects the rotated polarization into its basis and, as it is rotated by 90° with respect to the first one, attenuates the beam intensity respectively.

4.1 Results

We investigated the $5P_{3/2} \rightarrow 8D_{5/2}$ transition in Rubidium as the ESFADOF transition, which offers several advantages: (1) Its central wavelength of 543.3 nm lies close to the absorption minimum of water ([7]). (2) The radiation can be generated by second harmonic generation from the output of the fiber amplifier described in section 3 operating at 1086.6 nm. (3) The $5P_{3/2}$ state, which is the lower ESFADOF state, can be populated via the Rb D2 transition, $5S_{1/2} \rightarrow 5P_{3/2}$, by the radiation of a seeded tapered amplifier operating at 780.24 nm. Tapered amplifiers represent an easy to handle and low power consuming unit. As already reported in some of our earlier publications ([8,10,12]), the number density of the lower ESFADOF state, in our case the $5P_{3/2}$ state, has an enormous influence on the dispersion throughout the gas cell and therefore on the achievable maximum transmission of the filter. The population of the lower ESFADOF state can be actively controlled by the injected pump laser intensity. Therefore, as tapered amplifiers intrinsically offer rather bad beam profiles, care has to be taken in tailoring the beam profile of the pump laser. With the help of appropriate beam forming optics we managed to increase the available pump intensity by shrinking the beam diameter of our 500 mW output to 383 µm. The pump and the probe beams have been accurately overlapped. A power of 100 µW in the green distributed over a beam diameter of 233 µm was sufficient for recording the ESFADOF spectra.

Fig. 6 presents the ESFADOF spectra recorded at different cell temperatures and a constant magnetic field strength of 270 mT. The pump wavelength was held at the center of the Rb D2 transition. We can observe the following behavior: (1) Increasing the cell temperature increases the number density of the atomic gas and therefore the ESFADOF transmission. (2) The asymmetry of the transmission spectra is fully consistent to previously published measurements ([10]). However, the asymmetry is much more pronounced. Over the whole observed temperature range the red shifted part exhibits always higher transmission (up to a factor of 2) than the blue shifted part. (3) Beyond a cell temperature of 165°C the ESFADOF spectra exhibit much lower transmission. A further increase in temperature does not change the transmission anymore. (4) By slightly detuning the pump wavelength, as done in fig. 7, or by reducing the pump power the ESFADOF spectrum recovers again.

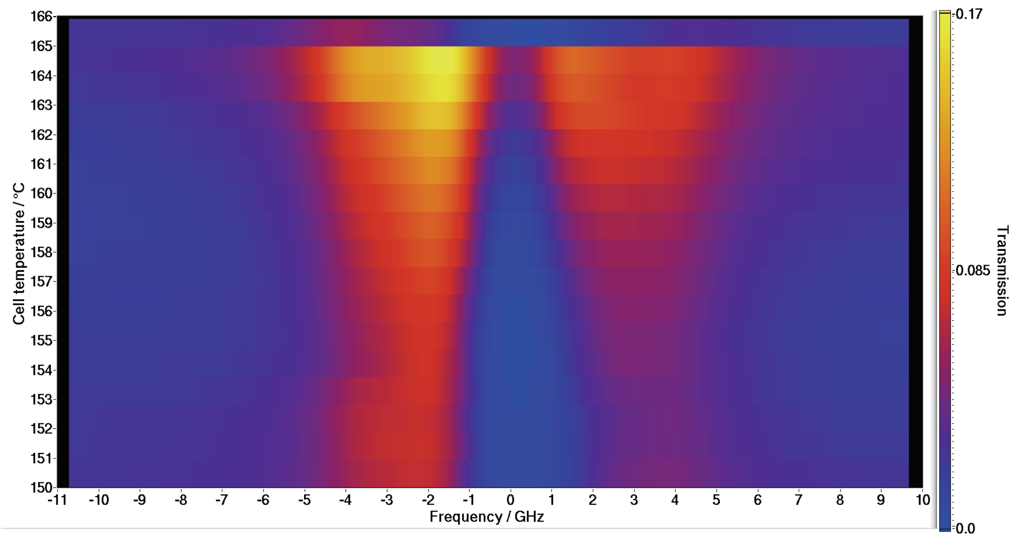

Figure 6: Variation of the ESFADOF cell temperature: By increasing the cell temperature one observes a clear dependency on the maximum ESFADOF transmission. This behavior is strongly correlated to the simultaneously increasing number density of the Rb gas in the cell. The pump wavelength has been placed on the center of the pump transition. The magnetic field strength is the same as in fig. 7. A concentration of the lower ESFADOF state population in favor of the red shifted peak can be observed. Striking is the existence of an upper temperature threshold at 165°C limiting the achievable maximum transmission. Beyond this temperature the maximum ESFADOF transmission reduces to barely 5% and remains constant while increasing the temperature. The zero on the frequency axes marks 543.3 nm.

The breakdown of the ESFADOF spectra can be explained by non-linear radiation-trapping ([29,30]) and energy-pooling processes ([31]). It will be investigated in a future publications more closely ([32]). Here we only briefly summarize: Whenever the intensity of the trapped photons reaches the saturation limit, radiation diffuses by stimulated emission significantly beyond the boundaries of the pumped volume. The stimulated emission process consumes the population on the $5P_{3/2}$ state much faster than the naturally observed decay rates in high density vapors. ([33]). In a second step, the additional radiation emerging from the energy-pooling process is also trapped and therefore affects another part of the available Rb atoms.

As soon as the trapped radiation drops below the saturation limit by means of reducing the pump power or the spectral overlap between the pump beam and the absorption lines, the diffusion process of the radiation trapping by stimulated emission collapses and the ESFADOF spectra recover. Fig. 7 shows such an ESFADOF spectrum for a cell temperature of T=167°C, a magnetic field strength of B_z=270 mT, a pump power of P_{Pump}=460 mW and a pump detuning of $\Delta\nu_{Pump}$=-5.78(2) GHz from the D2 transition center. The peak locations of the red and blue shifted transmission peaks are shifted towards the outside, compared to fig. 6. Therefore there is a significant redistribution of the $5P_{3/2}$-state population caused by the pump detuning. More precisely, the maximum peak transmissions in fig. 6 for T=165°C are located at -1.653(6) GHz and +1.581(6) GHz for the red and blue shifted peaks respectively, whereas in fig. 7, the maximum transmission shifts towards the outside of the spectrum. The red and blue shifted peaks can be found at -3.888(6) GHz and +4.336(6) GHz respectively.

Compared to the spectrum reported at the 3rd EARSeL worksop in 2007 ([12]), which is the inset of fig. 7, the maximum transmission increased by a factor of 3 and both peaks gain in transmission, structure and width. The red shifted peak shows a maximum transmission of 15.68(1)%, whereas the blue one contributes only with 6.04(1)%. Leaving the dips on the top of the peaks aside, one can assign a FWHM of 4.23(6) GHz and of 6.03(6) GHz for the red and blue shifted peaks respectively.

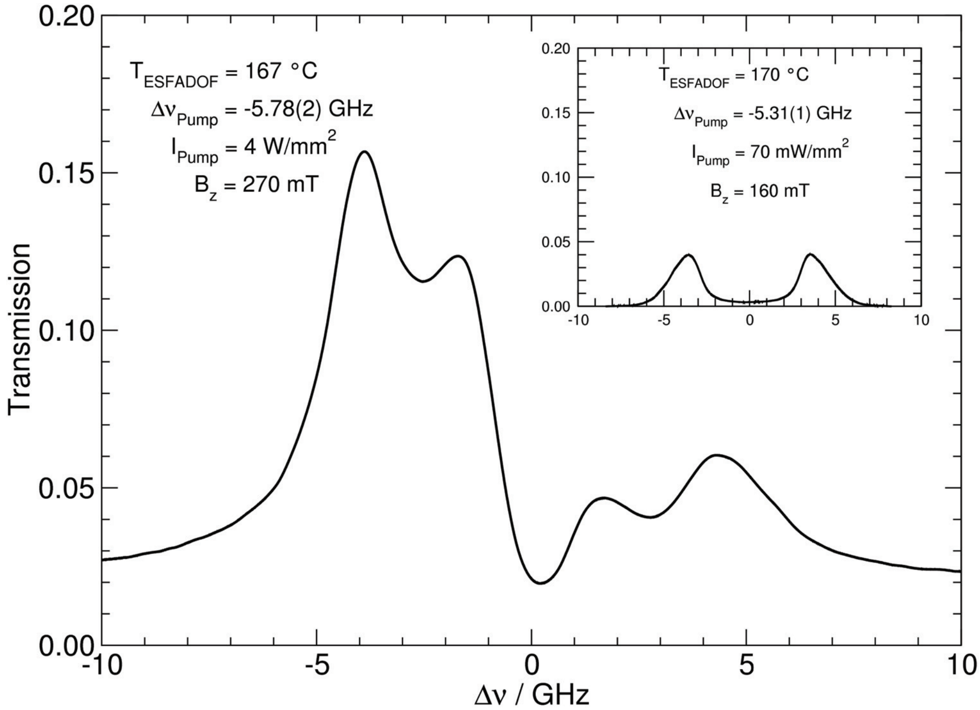

Figure 7: By slightly detuning the pump wavelength by $\Delta\nu_{Pump}$=-5.78(2) GHz the ESFADOF spectrum appears again. The inset shows the one reported at the 3rd-EARSeL workshop in 2007 ([12]). It is obvious, that edge filter characteristics increased significantly in transmission. The red peak by more than a factor of 3 and the blue one only slightly. Both peaks gain in structure and width. Leaving the dips on the top of the peaks aside, one can assign a FWHM of 4.23(6) GHz and of 6.03(6) GHz for the red and blue shifted peaks respectively.

The presented ESFADOF spectra prove that steep transmission edges are achievable with our set-up. Although the presented ESFADOF-set-up is still restricted in magnetic field strength, limiting the separation of the ESFADOF transmission edges, it does not discard the measurement scheme in principle. A more compact cell design will increase the magnetic field strength. In particular, the significant increase in the achieved transmission marks a milestone on the way to a practical system.

5 CONCLUSION AND OUTLOOK

In this paper we report data proving that spatially resolved temperature measurements employing the Brillouin lidar technique are feasible. Measurement from greater depths can be simulated by reducing the energy sent into the water. We estimate a potential operation depth of up to approximately 20 m depending on water quality with the currently available laser power and detection efficiency. Experiments to increase the laser power by employing polarization maintaining photonic crystal fibers ([34]) are currently under way. They are promising tools in increasing the second harmonic laser power, since they combine intrinsic single mode operation with excellent polarization maintaining capabilities.

The Fabry Perot interferometer has been used to proof the feasibility of our approach. It is clear that on-board an aircraft, the detection scheme has to be changed towards a mechanically stable edge filter. Our current efforts concentrate in changing the detection scheme to the presented excited state Faraday anomalous optical filter (ESFADOF). Furthermore, the edge filter technique will enable us to instantaneously measure a temperature profile and thus will utilize the laser pulses more efficiently ([10]). The operating wavelength of the fiber amplifier can be easily matched to the requirements of the ESFADOF.

ACKNOWLEDGMENTS

This work is supported in part by the state of Hessen and the DFG within the framework of the Graduiertenkolleg GRK 1114.

REFERENCES

1 J. Guagliardo and H. Dufilho, „Range-resolved Brillouin scattering using a pulsed laser“, Rev. Sci. Instr. 51, 79-81 (1980).

2 E. Fry, Y. Emery, X. Quan, and J. Katz, „Accuracy limitations on Brillouin LIDAR measurements of temperature and sound speed in the ocean“, Appl. Opt. 36, 6887-6894 (1997).

3 Y. Emery and E. Fry, „Laboratory development of LIDAR for measurement of sound velocity in the ocean using Brillouin scattering“, Proc. SPIE, Ocean Optics XIII 2963, 210-215 (1996).

4 E. Fry, J. Katz, R. Nicolaescu, and T. Walther, „Remote Sensing in the Ocean: Measurement of Sound Speed and Temperature“, Proc. SPIE, Ocean Optics XIV (1998).

5 E. Fry, J. Katz, D. Liu, and T. Walther, „Temperature dependence of the Brillouin linewidth in water“, J. of Mod. Opt. 49, 411-418 (2002).

6 G. Hickman, J. Harding, M. Carnes, A. Pressman, G. Kattawar, and E. Fry, „Aircraft Laser Sensing of Sound Velocity in Water: Brillouin Scattering“, Rem. Sens. Environ. 36, 165-178 (1991).

7 R. Pope and E. Fry, „Absorption spectrum (380-800 nm) of pure water. II. Integrating cavity measurements“, Appl. Opt. 36, 8710-8723 (1997).

8 A. Popescu, K. Schorstein, and T. Walther, „A Novel Approach to a Brillouin-LIDAR for Remote Sensing of the Ocean Temperature“, Appl. Phys. B 79, 955-961 (2004).

9 A. Popescu and T. Walther, „On the Potential of Faraday Anomalous Dispersion Optical Filter as High-Resolution Edge Filters“, Laser Phys. 15, 55-60 (2005).

10 A. Popescu, D. Walldorf, K. Schorstein, and T. Walther, „On an Excited State Faraday Anomalous Dispersion Optical Filter at Moderate Pump Powers for a Brillouin-LIDAR Receiver System“, Opt. Comm. 264, 475-481 (2006).

11 K. Schorstein, G. Scheich, A. Popescu, T. Walther, and E. S. Fry, „A Fiber Amplifier and an ESFADOF: Developments for a Transceiver in a Brillouin LIDAR“, Laser Physics 17, 975-982 (2007).

12 A. Popescu, K. Schorstein, G. Scheich, I. Massmann, P. Fietzek, T. Walther, and E. S. Fry, „Key Developments for a Brillouin-LIDAR for Remote Sensing of Oceanic Temperature Profiles“, in 3rd EARSeL Workshop on the Remote Sensing of the Coastal Zone, R. Reuter, ed. (2007).

13 M. Ulbricht (2005). Private communication. Adlares GmbH.

14 H. Pask, R. Carman, D. Hanna, A. Tropper, C. Mackechnie, P. Barber, and J. Dawes, „Ytterbium-Doped Silica Fiber Lasers: Versatile Sources for the 1-1.2 µm Region“, IEEE J. of Selected Topics in QE 1, 2-13 (1995).

15 R. Paschotta, J. Nilsson, A. Tropper, and D. Hanna, „Ytterbium-Doped Fiber Amplifiers“, IEEE J. of QE 33, 1049-1056 (1997).

16 E. Snitzer, H. Po, F. Hakimi, R. Tumminelli, and B. McCollum, „Double-clad, offset core Nd fiber laser“, in Optical Fiber Sensors, vol. 2 of OSA Technical Digest Series, p. PD5 (Optical Society of America, Washington D.C., 1988).

17 L. Zenteno, „High-Power Double-Clad Fiber Lasers“, J. of Lightw. Techn. 11, 1435-1446 (1993).

18 N. Broderick, H. Offerhaus, D. Richardson, R. Sammut, J. Caplen, and L. Dong, „Large Mode Area Fibers for High Power Applications“, Opt. Fiber Techn. 5, 185-196 (1999).

19 M.-Y. Cheng, Y.-C. Chang, A. Galvanauskas, P. Mamidipudi, R. Changkakoti, and P. Gatchell, „High-Energy and high-peka power nanosecond pulse generation with beam quality control in 200-µm-core highly multimode Yb-doped fiber amplifiers“, Opt. Lett. 30, 358-360 (2005).

20 O. Schmidt, J. Rothhardt, F. Röser, S. Linke, T. Schreiber, K. Rademaker, J. Limpert, S. Ermeneux, P. Yvernault, F. Salin, and A. Tünnermann, „Miilijoule pulse energy Q-switched short-length fiber laser“, Opt. Lett. 32, 1551-1553 (2007).

21 K. Schorstein and T. Walther, „A high spectral brightness Fourier transform limited nanosecond Yb-doped fiber amplifier“, Appl. Phys. B (2009). Submitted.

22 R. Nicolaescu, E. Fry, and T. Walther, „Generation of near-Fourier-transform-limited high-energy pulses in a chain of fiber-bulk amplifiers“, Opt. Lett. 26, 13-15 (2001).

23 G. Agrawal, Nonlinear Fiber Optics (Academic Press, 1995).

24 R. Smith, „Optical power handling capacity of low loss optical fibers as determined by stimulated Raman and Brillouin scattering“, Appl. Opt. 11, 2489-2494 (1972).

25 Y. Jaouën, G. Canat, S. Grot, and S. Bordais, „Power limitation induced by nonlinear effects in pulsed high-power fiber amplifiers“, C. R. Physique 7 (2006).

26 K. Schorstein, E. Fry, and T. Walther, „Depth resolved temperature measurements of water using the Brillouin-lidar technique“, Appl. Phys. B (2009). Submitted.

27 K. Schorstein, A. Popescu, M. Göbel, and T. Walther, „Remote Water Temperature Measurements Based on Brillouin Scattering with a Frequency Doubled Pulsed Yb: doped Fiber Amplifier“, Sensors 8, 5820-5831 (2008).

28 K. Schorstein, A. Popescu, G. Scheich, T. Walther, and E. Fry, „Towards a Brillouin-LIDAR for remote sensing of the temperature profile in the ocean“, OCEANS 2006 pp. 1-6 (2006).

29 T. Stacewicz, T. Kotowski, P. Wiewir, and J. Choräzy, „Diffusion of resonance radiation in opti-

cally saturated sodium vapour“, Opt. Comm. 100, 99 (1993).

30 J. Choräzy, T. Kotowski, and T. Stacewicz, „Investigation of resonance radiation trapping for optically saturated $3^2S_{1/2} \rightarrow 3^2P_{1/2}$ transition in sodium vapour“, Opt. Comm. 125, 65 (1996).

31 L. Barbier and M. Cheret, „Energy pooling process in rubidium vapour“, J. Phys. B.: At. Mol. Phys. 16, 3213-3228 (1983).

32 A. Popescu and T. Walther, Appl. Phys. B., to be published (2009).

33 T. Scholz, J. Welzel, and W. Lange, „Experiments on nonlinear radiation trapping in a saturable atomic vapor“, Phys. Rev. 64, 1 (2001).

34 C. Brooks and F. di Teodoro, „Multimegawatt peak-power, single-transverse-mode operation of a 100 µm core diameter, Yb-doped rodlike photonic crystal fiber amplifier“, Appl. Phys. Let. 89, 111,119 (2006).